CORA Cork Open Research Archive
Cartlann Taighde Oscailte Chorcaí

Title	All-optical technique for modulation format conversion from on-off-keying to alternate-mark-inversion
Authors	Dailey, James M.;Webb, Rod P.;Manning, Robert J.
Publication date	2010-10-10
Original Citation	Dailey, J.M., Webb, R.P., Manning, R.J. (2010) 'All-optical technique for modulation format conversion from on-off-keying to alternate-mark-inversion'. Optics Express, 18 (21):21873-21882. doi: 10.1364/OE.18.021873
Type of publication	Article (peer-reviewed)
Link to publisher's version	http://www.opticsinfobase.org/abstract.cfm?URI=oe-18-21-21873 - 10.1364/OE.18.021873
Rights	© 2010 Optical Society of America. This paper was published in Optics Express and is made available as an electronic reprint with the permission of OSA. The paper can be found at the following URL on the OSA website: http://www.opticsinfobase.org/abstract.cfm?URI=oe-18-21-21873 Systematic or multiple reproduction or distribution to multiple locations via electronic or other means is prohibited and is subject to penalties under law
Download date	2025-04-10 08:33:47
Item downloaded from	https://hdl.handle.net/10468/408

UCC
University College Cork, Ireland
Coláiste na hOllscoile Corcaigh

This paper was published in *Optics Express* and is made available as an electronic reprint with the permission of OSA. The paper can be found at the following URL on the OSA website:

http://www.opticsinfobase.org/oe/abstract.cfm?URI=oe-18-21-21873

Systematic or multiple reproduction or distribution to multiple locations via electronic or other means is prohibited and is subject to penalties under law.

All-optical technique for modulation format conversion from on-off-keying to alternate-mark-inversion

J.M. Dailey, R.P. Webb, and R.J. Manning
Tyndall National Institute & Department of Physics, University College Cork, Lee Maltings, Cork, Ireland
james.dailey@tyndall.ie

Abstract: We propose and numerically investigate for the first time a novel all-optical on-off-keying to alternate-mark-inversion modulation format converter operating at 40 Gbps employing a semiconductor optical amplifier (SOA)-based Mach-Zehnder interferometer (MZI). We demonstrate that this SOA-MZI operates as a pulse subtractor, and in the absence of patterning will produce perfectly phase inverted pulses regardless of the individual SOA phase excursions. We use a comprehensive computer model to illustrate the impact of patterning on the output phase modulation which is quantified through the definition of the phase compression factor.

© 2010 Optical Society of America

OCIS codes: (250.5980) Semiconductor optical amplifiers; (230.1150) All-optical devices; (060.4080) Modulation; (060.0060) Fiber optics and optical communication; (070.4340) Nonlinear optical signal processing

References and Links

1. P. J. Winzer, and R. J. Essiambre, "Advanced Optical Modulation Formats," Proceedings of the IEEE **94**, 952-985 (2006).
2. X. Zheng, D. Mahgerefteh, Y. Matsui, X. Ye, V. Bu, K. McCallion, H. Xu, M. Deutsch, H. Ereifej, R. Lewen, J. O. Wesstrom, R. Schatz, and P. J. Rigole, "Generation of RZ-AMI using a widely tuneable modulated grating Y-branch chirp managed laser," in *Conference on Optical Fiber Communication and National Fiber Optic Engineers Conference (OFC-NFOEC 2010)*, paper OThE5.
3. K. S. Cheng, and J. Conradi, "Reduction of pulse-to-pulse interaction using alternative RZ formats in 40-Gb/s systems," Photonics Technol. Lett. **14**, 98-100 (2002).
4. P. J. Winzer, A. H. Gnauck, G. Raybon, S. Chandrasekhar, Y. Su, and J. Leuthold, "40-Gb/s return-to-zero alternate-mark-inversion (RZ-AMI) transmission over 2000 km," Photonics Technology Letters, IEEE **15**, 766-768 (2003).
5. J. Yu, G. K. Chang, J. Barry, and Y. Su, "40 Gbit/s signal format conversion from NRZ to RZ using a Mach-Zehnder delay interferometer," Optics Communications **248**, 419-422 (2005).
6. W. Kaiser, T. Wuth, M. Wichers, and W. Rosenkranz, "Reduced complexity optical duobinary 10-Gb/s transmitter setup resulting in an increased transmission distance," Photonics Technology Letters, IEEE **13**, 884-886 (2001).
7. S. B. Jun, K. J. Park, K. Hoon, H. S. Chung, J. H. Lee, and Y. C. Chung, "Passive optical NRZ-to-RZ converter," in *Optical Fiber Communication Conference (OFC 2004)*, paper ThN1.

8. Q. Li, T. Ye, Y. Lu, Z. Zhang, M. Qiu, and Y. Su, "All-optical NRZ-to-AMI conversion using linear filtering effect of silicon microring resonator," Chin. Opt. Lett. **7**, 12-14 (2009).
9. G.-W. Lu, L.-K. Chen, and C.-K. Chan, "A simple AMI-RZ transmitter based on single-arm intensity modulator and optical delay interferometer," Optics Communications **255**, 35-40 (2005).
10. P. J. Winzer, and J. Leuthold, "Return-to-zero modulator using a single NRZ drive signal and an optical delay interferometer," Photonics Technology Letters, IEEE **13**, 1298-1300 (2001).
11. C. G. Lee, Y. J. Kim, C. S. Park, H. J. Lee, and C.-S. Park, "Experimental demonstration of 10-Gb/s data format conversions between NRZ and RZ using SOA-loop-mirror," J. Lightwave Technol. **23**, 834-841 (2005).
12. I. Kang, M. Rasras, L. Buhl, M. Dinu, S. Cabot, M. Cappuzzo, L. T. Gomez, Y. F. Chen, S. S. Patel, N. Dutta, A. Piccirilli, J. Jaques, and C. R. Giles, "All-optical XOR and XNOR operations at 86.4 Gb/s using a pair of semiconductor optical amplifier Mach-Zehnder interferometers," Opt. Express **17**, 19062-19066 (2009).
13. L. Billes, J. C. Simon, B. Kowalski, M. Henry, G. Michaud, P. Lamouler, and F. Alard, "20 Gbit/s optical 3R regenerator using SOA based Mach-Zehnder interferometer gate," in *11th International Conference on Integrated Optics and Optical Fibre Communications and 23rd European Conference on Optical Communications (IOCC-ECOC 1997)*, 269-272 vol.262.
14. J. M. Dailey, S. K. Ibrahim, R. J. Manning, R. P. Webb, S. Lardenois, G. D. Maxwell, and A. J. Poustie, "42.6 Gbit/s fully integrated all-optical XOR gate," Electronics Letters **45**, 1047-1049 (2009).
15. R. P. Webb, R. J. Manning, G. D. Maxwell, and A. J. Poustie, "40 Gbit/s all-optical XOR gate based on hybrid-integrated Mach-Zehnder interferometer," Electronics Letters **39**, 79-81 (2003).
16. T. Durhuus, B. Mikkelsen, C. Joergensen, S. Lykke Danielsen, and K. E. Stubkjaer, "All-optical wavelength conversion by semiconductor optical amplifiers," J. Lightwave Technol. **14**, 942-954 (1996).
17. I. Kang, C. Dorrer, L. Zhang, M. Rasras, L. Buhl, A. Bhardwaj, S. Cabot, M. Dinu, X. Liu, M. Cappuzzo, L. Gomez, A. Wong-Foy, Y. F. Chen, S. Patel, D. T. Neilson, J. Jacques, and C. R. Giles, "Regenerative all optical wavelength conversion of 40-Gb/s DPSK signals using a semiconductor optical amplifier Mach-Zehnder interferometer," in *31st European Conference on Optical Communication (ECOC 2005)*, 29-30 vol.26.
18. F. Koyama, and K. Iga, "Frequency chirping in external modulators," J. Lightwave Technol. **6**, 87-93 (1988).
19. R. D. Gitlin, J. F. Hayes, and S. B. Weinstein, *Data Communication Principles* (Plenum Press, New York, 1992).
20. J. M. Dailey, and T. L. Koch, "Simple Rules for Optimizing Asymmetries in SOA-Based Mach-Zehnder Wavelength Converters," J. Lightwave Technol. **27**, 1480-1488 (2009).
21. R. P. Webb, J. M. Dailey, and R. J. Manning, "Pattern Compensation in SOA-based Gates," Optics Express **18**, 13502-13509 (2010).
22. S. Bischoff, M. L. Nielsen, and J. Mork, "Improving the all-optical response of SOAs using a modulated holding signal," J. Lightwave Technol. **22**, 1303-1308 (2004).
23. O. Leclerc, B. Lavigne, E. Balmefrezol, P. Brindel, L. Pierre, D. Rouvillain, and F. Seguineau, "Optical Regeneration at 40 Gb/s and Beyond," J. Lightwave Technol. **21**, 2779 (2003).

1. Introduction

The non-return-to-zero on-off keying (NRZ-OOK) modulation format has been a traditional mainstay in telecoms networks due to the relatively small transceiver bandwidth required for its generation. The continually growing demand for higher network capacity, coupled with increasingly sophisticated electronic technology, has fueled research in advanced modulation formats [1]. The demand for capacity will probably be satisfied, at least in part, through the use of multi-level spectrally-efficient modulation formats such as quadrature amplitude modulation (QAM). However, these signaling schemes require sophisticated coherent receivers for detection, and as a result interest still remains in advanced OOK formats which can provide superior transmission performance while taking advantage of simpler direct detection receivers [2]. One such modulation format is alternate mark inversion (AMI) where OOK pulses, typically return-to-zero (RZ), are also phase modulated so that each pulse is phase-inverted with respect to its neighboring pulses [1, 2]. AMI differs from phase-shift keying in that information is not conveyed by the phase, but rather through the amplitude modulation. The correlated phase modulation enables, for example, suppression of ghost pulses and improvement in receiver sensitivity [3, 4].

With the maturation of advanced modulation format technologies, such as AMI, optical network designers will have greater flexibility in choosing optimized schemes, and as a result these future networks may incorporate disparate modulation formats requiring inter-format translators [5]. This translation can be accomplished using an optoelectronic receiver and rebroadcasting the data using a transmitter configured for the intended modulation scheme [1, 3, 6]. Alternatively, all-optical techniques can be utilized for these format conversions. All-optical methods generally employ ultrafast material nonlinearities and may scale more gracefully than their electronic counterparts to the high bitrates demanded of future networks. Semiconductor optical amplifiers (SOA) have generated particular interest as nonlinear elements due to their speed, size, and potential for integration.

There has been considerable work in the past on the all-optical conversion of NRZ to RZ signals, and though not necessarily the focus of the work, several of these techniques produced RZ-AMI outputs [5, 7-10] using passive filters. Such passive techniques are relatively simple to implement but suffer from limited regenerative abilities and have no wavelength conversion capability. Lee, *et al*, [11] demonstrated 10 Gbps all-optical format conversion with AMI output using a SOA-based loop mirror. This active approach enables wavelength conversion and has the potential for greater regenerative capabilities, but is limited in its bitrate scalability due to the strong dependence of the switching window on the single SOA's recovery time.

We numerically investigate for the first time, to our knowledge, an active SOA-based exclusive-or (XOR) gate approach. The XOR gate is constructed using a Mach-Zehnder interferometer (MZI) which can be configured to create switching windows much shorter than the SOA recovery time, and we focus on the all-optical conversion of input RZ-OOK to RZ-AMI pulses at a bitrate of 40 Gbps. In contrast to the previous work discussed above, this active approach offers a useful wavelength conversion, the potential for high-bitrate operation [12], and the promise of 2R and 3R regeneration [13]. A thorough treatment of regeneration is beyond the scope of this paper and we leave it to future work.

Following this introduction we discuss the basic operational principles of this modulation converter in Section 2. We use a comprehensive computer model in Section 3 to verify its effective operation and demonstrate the quality of the output phase modulation while identifying its relationship to SOA recovery time. Section 4 contains our concluding remarks, and finally in the Appendix we demonstrate mathematically how AMI modulation arises at the output.

2. Operational principles

In this section we introduce the basic operating principles of our proposed all-optical modulation format converter. The main component of the modulation converter is an SOA-based MZI configured as an exclusive-OR (XOR) logic gate [14, 15]. After describing the XOR functionality of the optical gate, we analyze its ability to generate phase-inverted pulses. We then identify the proper relationship between the two data sequences injected into the XOR input ports to produce an AMI-modulated output.

The XOR gate is shown in Fig. 1 inside the dotted box with two input ports: A and B. A continuous-wave (cw) probe at a wavelength of λ_{AMI} is injected into the interferometer input port and propagates through the two SOAs which are capable of changing both the amplitude and phase of the probe. The upper arm of the MZI also contains a static phase shifter with value φ_0 which controls the interference condition of the probe at the MZI output port. In the absence of the OOK data input (λ_{data}) and by setting the static phase shifter to π radians, the probe destructively interferes at the MZI output.

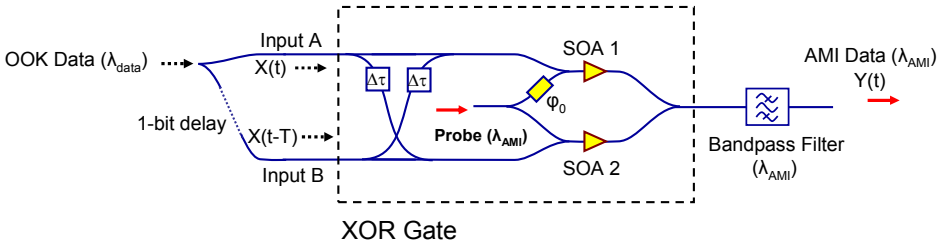

Fig. 1. The proposed all-optical modulation converter with the XOR gate shown inside the dotted box.

The XOR gate is shown in the push-pull configuration allowing switching windows much shorter than the SOA recovery times [14, 15]. A pulse injected into Input A is split between SOA1 and SOA2. A pulse first saturates SOA1, and the cross-gain (XGM) and cross-phase modulation (XPM) [16] processes disrupt the destructive interference of the probe at the output and the rising edge of a pulse at λ_{AMI} is created. The other pulse copy is delayed by $\Delta\tau$ seconds (less than a bit period) and enters SOA2 to close the switching window opened by SOA1. This creates the falling edge of the output pulse at the probe wavelength. Though the push-pull configuration enables the creation of short output pulses, it does not eliminate output patterning due to the finite recovery times of the SOAs.

The gate works in the same way for Input B though the SOAs are optically addressed in opposite sequence. If a pulse is inputted to both A and B the simultaneous phase excursions in the two SOAs cancel and the switch stays closed. In this way the MZI exhibits XOR functionality and we have recently demonstrated a 42.6 Gbps hybrid-integrated device operating with a low bit-error rate penalty [14]. Fig. 3 in Section 3 provides a visual reference for the various optical signals and depicts the SOA inputs, the XPM shifts on the probe, and the MZI output.

Kang, *et al*, have previously pointed out in [17] that SOA-MZIs are capable of all-optically generating phase inverted pulses. We analyze this switching behavior in further detail here using a transfer function analysis of the XOR gate. The electric field output from the XOR gate, $\vec{E}_{out}$, can be written as

$$\vec{E}_{out} = \vec{E}_{in} \cdot H\left(\varphi_{SOA1}, \varphi_{SOA2}\right) \tag{1}$$

where $\vec{E}_{in}$ is the electric field of the probe input to the gate and H is the gate's transfer function which changes depending on the input OOK data. φ_{SOA1} and φ_{SOA2} are the phase shifts induced on the probe by SOA1 and SOA2, respectively. For the sake of clarity, in calculating H we neglect the pull inputs (i.e. the $\Delta\tau$ delayed inputs in Fig. 1) as well as the XGM on the probe and utilize the MZI expression [18]

$$H(\varphi_{SOA1},\varphi_{SOA2}) = e^{j\left(\frac{\pi+\varphi_{SOA1}+\varphi_{SOA2}}{2}\right)} \cdot \sin\left(\frac{\varphi_{SOA2}-\varphi_{SOA1}}{2}\right) \tag{2}$$

where the static phase shift, φ_0, is set to π radians. Our conclusions based on H, which in Eq. (2) omits XGM and the pull inputs, are later validated in Section 3 where the complete numerical model includes both details.

H becomes nonzero after one of two input states: (1,0) or (0,1) where (A,B) are the binary inputs to ports A and B. For example, input state (1,0) describes a pulse inputted to SOA1 while no pulse is inputted into SOA2. This leads to a nonzero phase shift only in SOA1 and as a result $\varphi_{SOA1} < 0$ and $\varphi_{SOA2} = 0$. Using Eq. (2) we can compare the output electric fields resulting from input states (1,0) and (0,1) as

$$\frac{\vec{E}_{in}\cdot H(\varphi_{SOA1},0)}{\vec{E}_{in}\cdot H(0,\varphi_{SOA2})} = \frac{\vec{E}_{in}\cdot e^{j\left(\frac{\pi+\varphi_{SOA1}}{2}\right)}\cdot\sin\left(\frac{-\varphi_{SOA1}}{2}\right)}{\vec{E}_{in}\cdot e^{j\left(\frac{\pi+\varphi_{SOA2}}{2}\right)}\cdot\sin\left(\frac{\varphi_{SOA2}}{2}\right)} = \frac{-\sin\left(\frac{\varphi_{SOA1}}{2}\right)}{+\sin\left(\frac{\varphi_{SOA1}}{2}\right)} = -1. \tag{3}$$

In computing Eq. (3) we assume that φ_{SOA1} in the numerator and φ_{SOA2} in the denominator are equal in value. Eq. (3) indicates that with this assumption the two nonzero output fields are π radians out of phase with each other.

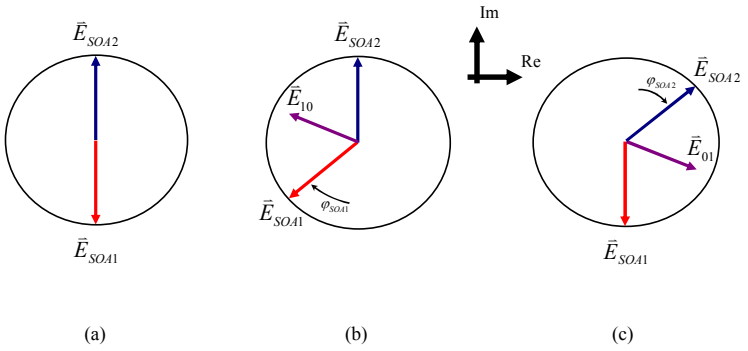

Fig. 2. Electric field phasor diagrams depicting the two SOA output field vectors, $\vec{E}_{SOA1}$ and $\vec{E}_{SOA2}$, and the relative orientation between the two possible output fields, $\vec{E}_{10}$ and $\vec{E}_{01}$.

The result captured in Eq. (3) can also be visualized using the phasor diagrams in Fig. 2. Fig. 2a shows the electric field outputs from both SOAs. $\vec{E}_{SOA1}$ is the field output from SOA1 and is shown equal in amplitude to the field output from SOA2, $\vec{E}_{SOA2}$, and with a π

phase shift due to the static phase shifter φ_0. The vector sum of these fields at the output of the interferometer is zero. When a pulse enters SOA1, i.e. input state (1,0), the XPM on the probe rotates $\vec{E}_{SOA1}$ clockwise by φ_{SOA1} radians as shown in Fig. 2b, and the vector sum of the fields is labeled as $\vec{E}_{10}$. As SOA1 recovers, $\vec{E}_{SOA1}$ rotates back to its original orientation and the interferometer closes. Likewise, when a pulse enters SOA2, i.e. input state (0,1), $\vec{E}_{SOA2}$ is rotated by φ_{SOA2} radians in the clockwise direction as shown in Fig. 2c. The resultant output field is labeled as $\vec{E}_{01}$. When φ_{SOA1} and φ_{SOA2} are equal, $\vec{E}_{10}$ and $\vec{E}_{01}$ have the same amplitude and are π radians out of phase with respect to each other. Ideal XOR gate operation is summarized in Table 1 where the input and output are represented by digital values.

Table 1. Optical XOR Logic

A (λ_{data})	B (λ_{data})	A XOR B † (λ_{AMI})
0	0	0
0	1	-1
1	0	1
1	1	0

† A XOR B can be written as (A-B)

We stress the important result from Eq. (3) that the phase inversion between the two output fields is realizable even if the individual phase excursions, φ_{SOA1} and φ_{SOA2}, are unequal to π radians. If the gate's static phase shift is set to π radians, then it is only necessary for the SOA phase excursions to be equal to ensure π phase shifts on the output fields. This suggests that this technique will work across the SOA gain bandwidth, possess a large input dynamic range, and be capable of optimization for a wide range of SOA operational conditions. However, we anticipate that pattern effects may cause pulse-to-pulse variations in φ_{SOA1} and φ_{SOA2} and break the necessary operational symmetry. We deal with this issue in detail later.

AMI is a linecode that can be generated using a 1-bit delay-and-subtract operation [1, 19] resulting in each output pulse having a phase inversion with respect to its two nearest-neighbors. This coding is often done in the electrical domain, but Table 1 indicates that the XOR gate effects the necessary field subtraction in the optical domain between its two input ports. This suggests that AMI modulation can be produced at the output by injecting the OOK data into one of the XOR inputs (*X(t)* at Input A in Fig. 1) and a copy of the data delayed by one bit period, *T*, into the other input (*X(t-T)* at Input B in Fig. 1). The output data *Y*(*t*) can be idealized as a modulated optical clock such that

$$Y(t) = \frac{1}{\sqrt{2}}\left[\vec{E}_{SOA2}(t) + \vec{E}_{SOA1}(t)\right] \approx \sum_{n=-\infty}^{\infty} y[n] \cdot u(t - nT) \tag{4}$$

where $y[n]$ and $u(t)$ are the digital output modulation and the field envelope of a single pulse, respectively. $y[n]$ can take any of three symbol values: {-1 0 1}. We show rigorously in the Appendix that upon inspection of any two successive output marks, $y[n]$ and $y[n+m]$, their relationship must be

$$y[n] = -y[n+m] \tag{5}$$

which is consistent with AMI modulation. In general, the encoding carried out by the XOR gate will result in an output digital message which differs from the input. The original message, i.e. the input binary sequence $x[n]$ to the converter, can be restored in a simple manner either through a precoding at the transmitter or decoding operation at the receiver [1, 19]. This precoding/decoding can in principle be carried out either electronically or all-optically.

The delay-and-subtract operation carried out by the XOR gate can be written as

$$y[n] = x[n] - x[n-1] \tag{6}$$

where y and x are taken as field quantities. Making use of the time-shift property of the Discrete Time Fourier Transform (DTFT) we can write the output spectral intensity as

$$\left|\widetilde{Y}(\omega)\right|^2 = \left|\widetilde{X}(\omega)\cdot\left(1-e^{-j\omega}\right)\right|^2 = 4\cdot\left|\widetilde{X}(\omega)\right|^2\cdot\sin^2\left(\frac{\omega}{2}\right) \tag{7}$$

where $\widetilde{X}$ and $\widetilde{Y}$ are the DTFTs of $x[n]$ and $y[n]$, respectively, and ω is the normalized frequency. The output spectrum from the XOR gate has nulls at the optical carrier frequency and multiples of the modulation bitrate as expected for an AMI scheme.

3. Numerical simulation and results

We now investigate the operation of the complete all-optical modulation converter, shown in Fig. 1, using a computer model based on a typical travelling-wave rate-equation analysis. The coupled partial differential equations are solved using a fourth-order Runge-Kutta algorithm. The XGM and XPM on the probe are captured via gain and refractive index changes which are calculated using a density matrix approach which eliminates the need for an α-factor approximation. Ultrafast effects are captured through carrier heating calculations. Further details can be found in [20].

The SOAs are 2mm long devices with high confinement factors of 0.54. Typical modeling parameters are utilized [20], and a bias current of 350 mA produces a gain peak of 30 dB centered at 1548 nm. Input powers should be above the 3-dB saturation input power of -19 dBm for good nonlinear performance. The gain recovery time is ~ 22 ps which is slightly smaller than the bit period at 40 Gbps. However, each SOA in the XOR gate can receive both a push and a pull (delayed by $\Delta\tau$) pulse, and the SOAs will not always have the full 25 ps bit period to recover. As a result, we expect more severe patterning on the output of this XOR gate than for a similar gate operating, for example, as an AND gate [14] or wavelength converter. We investigate patterning and its impact on operational speed later in this section.

The cw probe and data wavelengths are situated on the ITU grid at 1549.32 nm and 1548.51 nm, respectively. The total probe input power to the modulation converter is -7 dBm and the 3-dB splitter at the MZI input couples -10 dBm into each SOA. The 40 Gbps OOK input data are composed of 3 ps optical pulses with an average power of -4.2 dBm (2.8 mW peak power) which are modulated with a standard 2^7-1 pseudo-random binary sequence (PRBS). The push/pull power splitters shown in Fig. 1 are chosen to have a splitting ratio of ~ 70/30 to enable a good switching window [20]. The resulting push and pull input peak powers into each SOA are 1 mW and 0.4 mW, respectively. The $\Delta\tau$ delay built into the pull optical path is 8 ps, and the static phase shifter is set to π radians. The output sequence from the XOR gate will be the same PRBS due to the sequence's special properties.

The push and pull data input signals to the two SOAs are shown in the top two plots in Fig. 3. These plots show power as a function of time in units of bit number. The pull pulses input to SOA2 are clearly delayed copies of the push pulses input to SOA1. The third plot shows the probe phase shifts after the two SOAs, and the resulting switching windows. The bottom plot in Fig. 3 shows the output from the MZI gate and in order to display the ~ π phase shifts on the output signal, a phase reference is first chosen that orients the output field, i.e. *Y(t)*, along the real axis of the complex plane. The bottom plot shows the output power multiplied by the sign of the real part of the output electric field. The pulse-to-pulse phase changes are then shown as inversions around the zero level. We observe the phase changes to be consistent with AMI modulation.

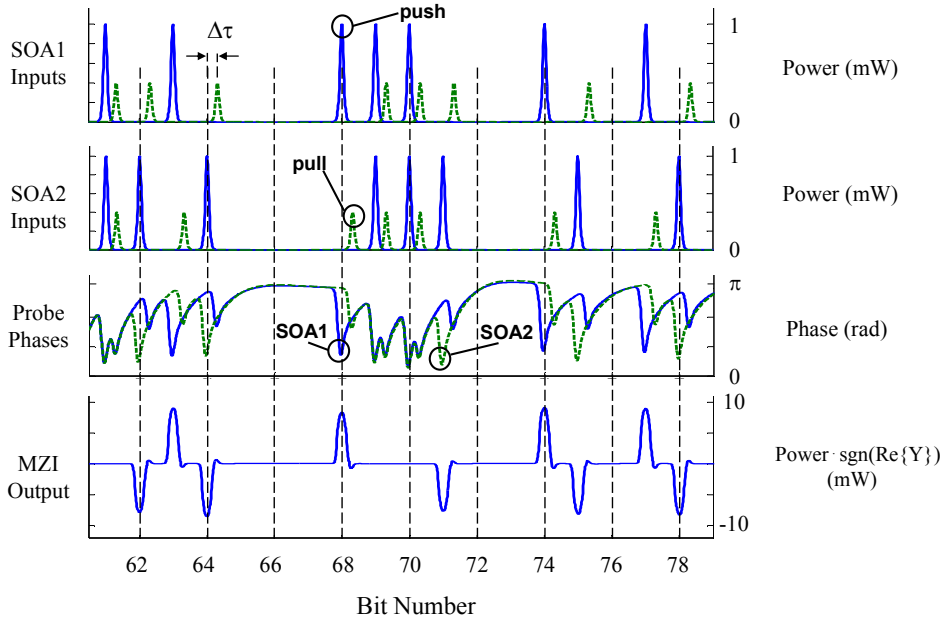

Fig. 3. Data inputs to SOA1 and SOA2 are shown in the first and second plots, respectively. The probe phase evolutions after the two SOAs are shown in the third plot with the static π phase shift removed for clarity. The MZI output pulses from the modulation converter are depicted in the fourth plot with the pulse phase changes shown as inversions around the zero level.

In this numerical experiment the SOA response time is comparable to the bit period and as a result the amplifiers are not completely recovered between data pulse excitations. This leads to patterning, or pulse-to-pulse amplitude and phase variations, and incomplete compliance with the conditions set forward in Eq. (3), i.e. that the two phase shifts should be equal to produce output pulses with π phase shifts.

In order to visualize both the amplitude and phase of the output signal, the electric field is sampled at the center of each of the 2^7-1 bit slots and these vectors are plotted as points in the complex plane making a constellation diagram. The field amplitudes have been normalized to lie near the unit circle. The two subsets of marks of opposing phase are clearly distinguished on this plot. The output pulse amplitude and phase patterning manifest as spreading in vector length and angle, respectively.

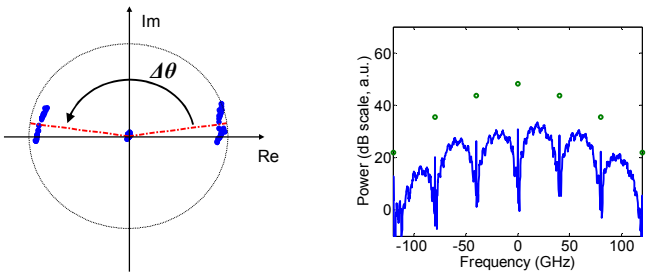

(a) (b)

Fig. 4. (a) Constellation diagram of the 40 Gbps output from the modulation converter. (b) The signal output spectrum (solid line) as well as carrier and sideband peaks (circles) with output phase modulation removed for comparison.

As expected, within each cluster of marks, Fig. 4a shows a spread in angle of the output samples corresponding to patterning. Additionally, the overall mean angular separation between the clusters is not equal to π radians. For each cluster of marks a line can be drawn with an angle that coincides with the samples' mean angle. These lines are shown as dash-dotted lines in Fig. 4a. The acute angle formed by these two lines is defined as $\Delta\theta$ and is shown in Fig 4a. We define the phase compression, δ, on the output signal as

$$\delta \equiv 1 - \frac{\Delta\theta}{\pi} \tag{8}$$

and offer δ as a metric for the efficacy of the modulation converter. The model predicts a phase compression of 9% for this modulation converter operating at 40 Gbps.

The source of the phase compression lies in the finite SOA recovery time. An output pulse from the converter occurs in one of two input scenarios: (1,0) and (0,1) where (A,B) are the input bits to ports A and B. Input port B receives the delayed data, and as a result on every occurrence of input condition (0,1), a pulse must have *necessarily* been input to port A in the immediately preceding bit period. This means that the switch can never be in a completely recovered state on input condition (0,1), and the resultant output pulses will have less of an average phase shift than their counterparts for input condition (1,0). The result is a phase angle between the two groups of output pulses which is not equal to π, i.e. phase compression.

The absence of the carrier frequency and bitrate harmonics is a characteristic of AMI modulated signals, see Eq. (7). This spectral suppression is related to some of the advantages over conventional unipolar OOK, and we expect that the two mark clusters in Fig 4a should be separated by π radians and each have small variances to achieve the best spectral rejection. The baseband AMI output spectrum is shown in Fig. 4b as the solid line. The circles plotted above this line show the height of the carrier and modulation sidebands for the output spectrum when the phase modulation is removed. This allows comparison of the spectra in the case of the desired output AMI modulation and the simpler unipolar OOK modulation. The plot shows that for a phase compression of 9% the AMI carrier is suppressed by > 17 dB with respect to the OOK carrier. Furthermore, the AMI carrier and bitrate harmonic frequencies are suppressed to roughly at or below the overall signal spectral envelope.

These results indicate the importance of the SOA recovery time relative to the bit period, and we expect better performance from this modulation converter as the recovery time is reduced with respect to the bit period. Specifically, we anticipate a reduction in the phase compression as well as better carrier and sideband extinction on the output spectrum.

We test this hypothesis by repeating the previous numerical experiment with identical parameters except the bit period is doubled from 25ps to 50ps, effectively lowering the input bitrate to 20 Gbps. The longer bit period allows the SOAs more time to recover and should greatly mitigate the parasitic pattern effects. The results from this simulation are shown in Fig. 5.

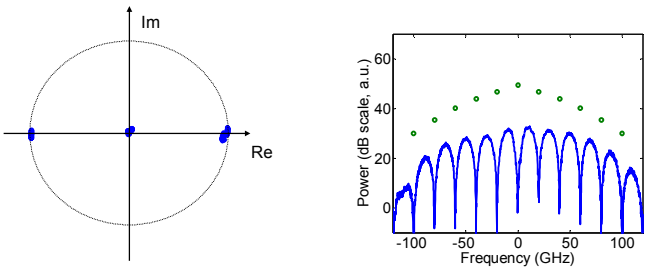

(a) (b)

Fig. 5. (a) Constellation diagram of the 20 Gbps output from the modulation converter. (b) The signal output spectrum (solid line) as well as carrier and sideband peaks (circles) with output phase modulation removed for comparison.

The constellation diagram of the 20 Gbps data output shown in Fig. 5a clearly demonstrates an increase in the quality of phase modulation including a much smaller phase compression measured to be 1%. The mark-cluster variance is smaller, as compared with Fig. 4a, indicating a lower degree of patterning. The output spectrum shown in Fig. 5b also demonstrates the higher quality of modulation through the stronger suppression of the carrier and bitrate harmonics. Furthermore, we note that the modeling indicates that the XPM shifts induced on the probe are all less than π radians and Fig 5 indicates that the pulse-to-pulse phase shifts are very close to π. This is consistent with the analysis given in Section 2.

These results clearly illustrate the impact that the finite SOA recovery time has on the quality of the output phase modulation. As suggested by the 20 Gbps experiment, this impact can be minimized by ensuring that the input bit period is much longer than the recovery times of the SOAs. We expect this recovery time requirement to be more severe than for an MZI wavelength converter of similar architecture (i.e. an AND gate) operating at the same bitrate due to the increased excitation frequency of the SOAs in an XOR configuration [14]. This requirement will be difficult to fulfill at speeds above 40 Gbps, however, a compensation scheme whereby inverted data is co-injected into the SOAs [12, 21, 22] may be useful in reducing the patterning.

4. Conclusions

We have proposed and numerically demonstrated the use of an active SOA-based XOR gate for all-optical OOK to AMI modulation conversion. The technique is based on the intrinsic symmetries in the Mach-Zehnder interferometer and, in the absence of patterning, should produce pulses with perfect phase inversion regardless of the magnitude of the two equal SOA phase excursions. We used a comprehensive computer model to verify the converter's

operation and to illustrate the output phase compression due to pattern effects ultimately arising from the finite SOA recovery time. The model predicts a phase compression of 9% at 40 Gbps and a carrier suppression of greater than 17 dB. We anticipate many of the transmission benefits of AMI modulation to be maintained with such performance. Furthermore, we expect that improved modulation converter performance may be possible at 40 Gbps and even higher bitrates by modifying previously demonstrated pattern compensation schemes [12, 21, 22] .

The ability of this converter to produce phase-inverted pulses using SOA phase excursions which are less than π radians suggests that this device will possess generous tolerances to input pulse width, power, and wavelength. We also anticipate that this active approach will compare favorably to previously demonstrated passive techniques due to its potential for 2R and 3R regeneration [13, 23]. Finally, our previous work with integrated XOR gates [14, 15] suggests that the optical split and 1-bit delay at the converter input can be readily incorporated using hybrid-integration technology.

Acknowledgment

This work was supported by Science Foundation Ireland under grant 06/IN/I969.

Appendix

We now provide a general mathematical treatment showing that the output from this modulator converter is AMI modulated for any arbitrary OOK input sequence. The input and output digital logic sequences are denoted as $x[n]$ and $y[n]$, respectively. Following the discussion in Section 2 where we noted that the XOR gate output is the difference between its inputs, we choose two output marks , i.e. logical "1"s, at index n and $n+m$ and write

$$\begin{aligned} y[n] &= x[n] - x[n-1] = \pm 1 \\ y[n+m] &= x[n+m] - x[n+m-1] = \pm 1 \end{aligned} \tag{9}$$

The index m is chosen so that $y[n+m]$ is the very next mark following $y[n]$ in the output sequence. There is some number of spaces, i.e. logical "0"s, between these marks and as a result

$$\begin{aligned} y[n+1] = 0 = x[n+1] - x[n] \quad &\rightarrow \quad x[n+1] = x[n] \\ y[n+2] = 0 = x[n+2] - x[n+1] \quad &\rightarrow \quad x[n+2] = x[n+1] = x[n] \\ \ldots \quad &\quad \ldots \\ y[n+m-1] = 0 = x[n+m-1] - x[n+m-2] \quad &\rightarrow \quad x[n+m-1] = x[n+m-2] = x[n] \end{aligned} \tag{10}$$

Because a mark can only emerge when the two inputs A and B (see Fig. 1) are complementary we can rewrite Eq. (9) as

$$y[n] = x[n] - x[n-1] = x[n] - \overline{x[n]}$$

$$y[n+m] = x[n+m] - x[n+m-1] = x[n+m] - x[n] = \overline{x[n]} - x[n] \tag{11}$$

where the results in Eq. (10) have been utilized. From Eq. (11) we conclude

$$y[n] = -y[n+m] \tag{12}$$

and because this argument is general, every mark is out of phase with the mark before and after it. This is consistent with AMI modulation.